Distance for communication between metal and acid sites

Yubing Li
Xiamen University
Mengheng Wang
Xiamen University
Suhan Liu
Xiamen University
Fangwei Wu
Xiamen University
Qinghong Zhang
Xiamen University https://orcid.org/0000-0001-6603-7656
Shuhong Zhang
Xiamen University
Kang Cheng (kangcheng@xmu.edu.cn)
Xiamen University https://orcid.org/0000-0002-7112-4700
Ye Wang
Xiamen University https://orcid.org/0000-0003-0764-2279

Article

Keywords: Tandem catalysis, communication, proximity, C1 chemistry, syngas

Posted Date: February 17th, 2022

DOI: https://doi.org/10.21203/rs.3.rs-1355935/v1

Abstract

Unraveling the proximity influence between different sites in tandem catalysis is particularly challenging. Herein, we evaluate the distance effect on the communication between metal and acid sites in a methanol-mediated syngas conversion system. A series of catalysts composed of $ZnZrO_x$ and zeolites with different proximity levels from millimeter- to nanoscale-scale were evaluated in the syngas to olefins (STO), gasoline (STG), and aromatics (STA) reactions. The distance requirements are dependent on the diffusivity of reaction intermediates and the formation mechanism of products. The STO and STG reactions follow a simple tandem mechanism, which is not sensitive to the distance as long as the gaseous methanol could fast diffuse to acid sites. Whereas a synergistic tandem mechanism for syngas to aromatics is evidenced, *i.e.*, the dehydro-aromatization step must be promoted by the intimate contact of metal and acid sites to eliminate the surface hydrogen species formed on zeolites.

Introduction

Tandem catalysis, which integrates two or more consecutive catalytic reactions in a single reactor, provides possibilities for creating new catalytic processes with better efficiencies[1–4]. It not only simplifies or even avoids the separation, purification, and transportation of reaction intermediates but also may make the overall reaction process more thermodynamically favorable and kinetically controllable[5]. In particular, tandem catalysis has recently reshaped the research pattern of C1 chemistry and allows the direct synthesis of C_{2+} high-value fuels and chemicals with ultrahigh selectivities (Fig. 1), *e.g.*, the transformation of syngas and CO_2 to liquid fuels, olefins, and aromatics[6–8], CH_4 dehydroaromatization[9,10], and oxidative coupling of CH_4[11]. One should note that concepts of tandem and bifunctional catalysis have overlaps and also differences. Tandem catalysis focuses on the reaction process while the bifunctional catalysis is weighted in the catalyst composition. A tandem process can be realized by bi- or multifunctional catalysts, but not all the tandem processes can be called bi- or multifunctional, *e.g.*, different catalyst components combined with dual- and triple-bed configurations[12–15].

Besides the compatibility of two functional sites, the reaction sequence must be executed in order and the intermediates must be consumed quickly for tandem catalysis, thus the distance between different functional sites also plays a crucial role in tandem processes (Fig. 1). To maximize the synergistic effect, it is generally agreed that a close distance between different sites is preferred[16,17]. However, several groups recently reported that for the typical bifunctional metal-zeolite catalysts, separating metal and acid sites with nanoscale or even microscale distance outperformed the catalysts with intimate distance in the alkane and syngas conversions[18–21]. The distance-dependent performances in heterogeneous catalysis have been often analyzed from the aspects of the accessibility of functional sites, the local concentration of intermediates, and the transfer mechanism[22–24]. It is noteworthy that because of the complicated formulations of bi- and multi-functional catalysts for tandem processes, a solid-state reaction between transition metals and zeolites may take place and strongly affect the catalytic

performances[25,26]. Sometimes, this phenomenon was mistakenly assigned to the proximity effect. A comprehensive understanding of the distance-induced optimum performance is necessary for the rational arrangements of functional sites for specific catalytic processes. However, up to now, deep investigation and understanding into the distance factor for tandem catalysis are still lacking.

Since the discovery of bifunctional oxide-zeolite catalysts for converting syngas into lower olefins in 2016[27,28], tremendous progress has been made in the selective transformation of syngas and CO_2 into aromatics, liquid fuels, and even single product, *e.g.*, ethylene, ethanol, and para-xylene[29–33]. To date, the protocols for the spatial organization of bifunctional components not only include an elegant core-shell structure with metal oxide encapsulated inside zeolites[34–37], but also a granule-mixing method with hundreds of microns between different sites and even dual-bed mode with millimeter-scale distance[20,38–41]. Generally, proximity has been recognized as an important factor for achieving ideal tandem catalysis but has not been investigated quantitatively based on different catalytic systems.

Herein, we investigate the distance impact on the emerging STO, STG, and STA tandem reactions achieved by oxide-zeolite catalysts. The distance between $ZnZrO_x$ for methanol synthesis and zeolites for C – C coupling was controlled from millimeter- to nanoscale-scale, and was semi-quantitatively estimated. We found that the distance requirement for sufficient communication in these tandem reactions is quite different, depending on the diffusivity, stability, and transfer mechanism of reaction intermediates, and the formation mechanism of desired products. The Péclet (*Pe*) number was employed to assess the back-mixing degree, which can also be understood as to how far the gaseous methanol intermediate can diffuse upstream to find acid sites. Furthermore, we first propose and establish a simple tandem and a synergistic tandem mechanism over the fast-growing oxide-zeolite catalysis.

Results

Effect of distance on catalytic performance

A binary $ZnZrO_x$ oxide was employed as the function for syngas to methanol under high temperature[28]. SAPO-34, SAPO-11, and H-ZSM-5 with optimized acidity and structure (Supplementary Figs. 1 – 3 and Supplementary Table 1) were used to perform C – C coupling[42–44]. A series of integration manners were used to tune the distance between $ZnZrO_x$ and zeolites from millimeter- to nanoscale-scale (Fig. 2a). For the granule-stacking and powder-mixing manners, the distance was semi-quantitatively estimated by an iterative method (Fig. 2b, Supplementary Fig. 4, and Supplementary Table 2). The distance between the two functional granules was found to be close to the sum of two radii because each granule could be considered as a matrix of active sites. One should note that the studies on the distance effect are often disturbed by the interaction of metal migration between the metal oxide and zeolites due to the harsh reaction conditions[25,26]. To exclude this effect, $ZnZrO_x$ with a low zinc content (Zn/Zr ratio ≤ 1/8) and stable structure was employed to conduct syngas to methanol reaction[45]. Without the detrimental effect of metal migration, all three sets of catalysts exhibited distance-dependent performance in syngas

conversion (Fig. 2c – e). Generally, the closer distance between metal and acid functions, the higher CO conversion and product selectivity were obtained for three tandem reactions.

Because of kinetic reasons, the C – C coupling over zeolites has to be conducted above 350 ^{o}C to avoid fast coking[46]. At such high temperatures, the methanol synthesis is thermodynamically limited, but the formation of hydrocarbons is much more favorable (Supplementary Fig. 5). Therefore from the perspective of kinetics, the communication between metal oxides and zeolites via methanol intermediates must be sufficient enough to drive the CO conversion over $ZnZrO_x$. The CO conversion levels over $ZnZrO_x$ with different Zn/Zr ratios were lower than 2.0% because of thermodynamic restriction (Fig. 2c – e and Supplementary Tables 3 – 5). The typical millimeter-scale fixed-bed reactor is often considered as a plug-flow reactor with little or no back-mixing of the flowing gas stream[47]. However, an unconventional integration manner with the zeolite in the upstream bed and $ZnZrO_x$ in the downstream bed (the second manner in Fig. 2a) showed that the conversion of syngas over $ZnZrO_x$ was significantly disturbed by zeolite (the second catalyst in Fig. 2c – e), even the thickness of the quartz wool in-between was 3 mm. The CO conversion was increased more than double, and the product shifted to hydrocarbon or dimethyl ether (DME) at the expense of methanol. These results suggest that the back-mixing effect could not be excluded and there existed communication between metal and acid sites even there are separated with a millimeter-scale distance. Placing zeolites in the downstream bed (the third manner in Fig. 2a), which is a typical integration manner for tandem catalysis, further increased the CO conversion and shifted the product towards lower olefins, gasoline, and aromatics. The increase of CO conversion over $ZnZrO_x$/SAPO-34 was even one magnitude as that of over $ZnZrO_x$, which means the consumption of methanol downstream could greatly drive the CO conversion over $ZnZrO_x$. Besides, no methanol and DME were detected, suggesting these gaseous intermediates could always find the acid sites downstream for further conversion even with the existence of a millimeter-scale distance and without a well-defined spatial arrangement between metal and acid sites. This phenomenon might not be surprising because of the high diffusivity of methanol intermediates under high temperatures.

Diffusion range of reaction intermediate

Considering the low space velocities of syngas (normally ≤ 8,000 h^{-1}) in tandem processes,[7] the transport of methanol intermediates in a typical fixed-bed reactor might be diffusion-dominated. The back-mixing effect can be assessed by the Péclet number (*Pe*), a class of dimensionless numbers relevant in the study of transport phenomena in a continuum. It is defined as the ratio of the rate of advection of a physical quantity by the flow to the rate of diffusion of the same quantity driven by an appropriate gradient. A large *Pe* number indicates an advectively dominated distribution, and a small number indicates diffusive effects dominate over convective transport[48]. In the tandem metal oxide-zeolite systems, the *Pe* number can also be used to assess “how far the methanol intermediates can diffuse upstream against the syngas flow” (Fig. 3a). One should note that methanol could theoretically diffuse along with the syngas flow direction without limit if it is stable enough. The definition of diffusion range is a rough distance that a specific molecule can diffuse counter-currently in a fixed-bed reactor,

driven by its diffusivity. By considering all the parameters that may affect the *Pe*, a distance of 5 mm was obtained when assuming the *Pe* was 1 (Supplementary Table 6). This means a large fraction of methanol molecules formed on a $ZnZrO_x$ particle could diffuse upstream as far as 5 mm against the syngas flow. Thus, it is easy to understand even the zeolites were placed in the upstream bed of the reactor, the methanol could diffuse back for C – C coupling and drive the overall CO conversion (Fig. 2c – e).

Compared with the deep investigation on the formation mechanism of methanol over oxide surface and the C – C coupling over zeolites, those on engineering aspects, *e.g.*, mass transfer and back-mixing, are much less. According to the equation for calculating *Pe* number, we quantified the effects of two adjustable factors, *i.e.*, reactor radius and reactant space velocity, on the diffusion range of methanol upstream, assuming it forms on oxides under realistic reaction conditions (Fig. 3b). The back-mixing effect in principle can be relieved by decreasing the radius of reactors or increasing the space velocity. However, to lower the pressure drop and separation cost, catalyst granules cannot be very small and also the reactor diameter. Even the multichannel microreactors designed by Velocys and Avantium are millimeter-scale[49,50]. Besides, increasing the space velocity is hazardous to the single-pass CO conversion considering the activity of mixed oxides in CO conversion still needs to be improved. The diffusivity nature of reaction intermediates is also related to the temperature (Supplementary Fig. 6), and a higher temperature is beneficial to the diffusivity of methanol. It might be intuitive to consider that a lighter molecule diffuses farther than the heavier ones. This view is usually right, *e.g.*, H_2 and CO are more diffusive than methanol (Fig. 3c). However, because the diffusivity is also related to the diffusion volume of specific molecules (Supplementary Table 6), some heavier molecules (e.g., DME and benzene) may diffuse farther than methanol. These factors are often overlooked but have far-reaching effects on reactor and catalyst design.

Simple and synergistic tandem mechanism

Although all the three examples exhibited a “the closer the better” tendency, the sensitivity of three catalytic systems to distance from 3 mm to the nanoscale is quite different (Fig. 2c – e). Generally, for STO and STG processes, packing the $ZnZrO_x$ and zeolites together with no matter micron-scale or nanoscale distance, the catalytic performance is not sensitive to distance (last three manners in Fig. 2c and d). Relatively, the STA performance is more sensitive to the distance factor. Only when the two functional components were closely integrated and contacted, a considerable aromatics selectivity above 70% at a high CO conversion could be obtained. For STO tandem reaction, the $ZnZrO_x$ functions for the syngas to methanol ($CO + 2H_2 \rightarrow CH_3OH$), and the formation of lower olefins can be solely catalyzed by SAPO-34 ($2CH_3OH \rightarrow C_2H_4 + 2H_2O$). As long as the methanol intermediates can rapidly find the acid sites, the tandem process and thermodynamic pull could be well realized. Therefore, the STO reaction catalyzed by metal oxide and zeolite can be considered as a simple tandem reaction, because each catalytic function works independently and the gaseous methanol intermediates diffuse rapidly (Fig. 4a). The STG tandem reaction is similar to the STO reaction because the formation of gasoline-range hydrocarbons can be solely conducted by zeolite.

The formation of aromatic hydrocarbon from methanol is complicated, including dehydration of methanol to lower olefins ($2CH_3OH \rightarrow C_2H_4 + 2H_2O$), olefin oligomerization ($3C_2H_4 \rightarrow$ hexene), cyclization (hexene → cyclohexane), and dehydrogenation (cyclohexane → benzene + $3H_2$)[44]. Therefore, methanol is not the only intermediate. The last dehydrogenation step is often considered the rate-determining step and the formed hydrogen species on zeolites should be removed efficiently to promote the formation of aromatics.[51,52] Otherwise, the aggregated hydrogen species would catalyze the formation of undesired saturated alkanes by an H-transfer mechanism (Fig. 4b). Actually, hydrogen species is another kind of key reaction intermediates in STA tandem reaction, whose role was sometimes neglected. The transfer of methanol follows a gas diffusion mechanism, but that of hydrogen species normally follows a surface diffusion mechanism.[16,53] This might be the reason that the STA tandem reaction is quite sensitive to distance.

Transfer mechanism of reaction intermediates

To clarify the necessity of close distance/contact for optimum STA process, we delicately controlled the proximity between ZnO and H-ZSM-5 and performed model propylene aromatization reaction over typical ZnO/H-ZSM-5 catalyst under 5 bar and 390 ^oC (Fig. 5a). The pristine H-ZSM-5 exhibited a considerable C_3H_6 conversion of 79%, but the aromatics selectivity was only 33%, in line with the reported values.[54] To physically separate the ZnO and H-ZSM-5 components, we capsulated the ZnO nanoparticles (NPs) in a mesoporous SiO_2 shell with a thickness of 30 nm, which was further mixed with H-ZSM-5 powders (Supplementary Fig. 7). Interestingly, the performance of ZnO@SiO_2/H-ZSM-5 was close to that of H-ZSM-5, indicating no communication between ZnO and H-ZSM-5. However, if the ZnO NPs and H-ZSM-5 were closely in contact prepared by even a powder-mixing method, the aromatics selectivity could be significantly enhanced to 63% together with the formation of gaseous hydrogen (Supplementary Table 7), indicating a strong synergistic effect between ZnO and H-ZSM-5. This synergy could be further enhanced over ZnO-H-ZSM-5 prepared by an impregnation method with an intimate distance (Supplementary Fig. 8), providing the highest aromatics selectivity of 72% at C_3H_6 conversion of 97%.

The activation ability of hydrogen was further evaluated by the H_2-D_2 exchange (Fig. 5b). Interestingly, the pristine H-ZSM-5 without transition metals could activate H_2 and D_2 and catalyze the formation of HD, in line with reported results that zeolites with Brønsted acid sites could catalyze the hydrogenation reaction by heterolytic cleavage[55,56]. However, the formation rate of HD over ZnO was much higher than that over H-ZSM-5. It was early reported that the transfer of hydrogen species on zeolites follows a surface migration mechanism and the transfer can be fast and distant[57,58]. Therefore, we can speculate that the close proximity of ZnO to H-ZSM-5 could promote the recombination of H-adatoms species to form H_2 on ZnO transferred from H-ZSM-5.

Based on the above results, the network of syngas to C_{2+} hydrocarbons can be briefly outlined (Fig. 5c), and the extent of reaction progress is determined by the topology of acidic zeolites. The number of reaction steps for each product follows the order of lower olefins < gasoline < aromatics. For the

formation of the aromatics, methanol and olefinic hydrocarbons are not all the intermediates and the fast removal of surface hydrogen species is indispensable. The metal and acid sites must be organized closely at the nanoscale to guarantee sufficient communication, thus completing the multi-step tandem reactions. Besides, if the formation of side products and reaction intermediates is competitive, a rational arrangement of active components may decrease the formation of side products by fast-consuming reaction intermediates.

Discussion

In summary, the proximity requirement for different tandem reactions may be quite different, depending on but not limited to the diffusivity, stability, and transfer mechanism of reaction intermediates, and reaction conditions. We preliminarily quantified the distance between the metal oxide and zeolites and its impact on the communication in the tandem conversion of syngas. Most lab-scale fixed-bed reactors for syngas conversion are not ideal plug-flow reactors because the back-mixing effect could not be neglected. The high diffusivity of methanol intermediate determines the low sensitivity of the simple tandem reactions, such as syngas to lower olefins and C_5–C_{11} isoparaffins. Even the two functional components are separated with a millimeter-scale distance, the methanol molecules could find acid sites for further conversion due to the high diffusivities. Conversely, if a tandem reaction involves intermediates that must be transferred on the catalyst surface, the two functional sites must be integrated as closely as possible without chemical interaction. This work not only explains the various interaction manners employed up to now over oxide-zeolite catalysts but also guides the rational arrangements of functional sites and the design of reactor shapes for specific tandem reactions.

Methods

Materials

Pseudoboehmite (Al_2O_3, 72 wt%) was purchased from Beijing Reagents Company. Silica solution (30 wt%) and tetraethylammonium hydroxide (TEAOH, 25wt%) were purchased from Sigma-Aldrich. Orthophosphoric acid (H_3PO_4, 85 wt%), triethylamine (TEA, 99 wt%), *di-n*-propylamine (DPA, AR), aluminum isopropoxide (99 wt%), zirconium nitrate ($Zr(NO)_4{\cdot}5H_2O$), zinc nitrate ($Zn(NO)_2{\cdot}9H_2O$), citric acid, $NH_3{\cdot}H_2O$ (25 wt%), ethanol (AR) and tetraethoxysilane (TEOS, AR) were purchased from Sinopharm Chemical Reagent. H-ZSM-5 zeolite (a molar ratio of Si/Al = 200) was purchased from Nankai University Catalyst Company. The glassware was provided by Xiamen University Glassware Workshop.

Catalyst preparation

The Zn-doped ZrO_2 ($ZnZrO_x$) oxide for STG reaction was synthesized with a sol-gel method with a Zn/Zr ratio of 1:8 (at/at)[45]. Specifically, 10 g of $Zr(NO_3)_4{\bullet}5H_2O$, 0.87 g of $Zn(NO_3)_2{\bullet}6H_2O$, and 9.4 g of citric acid were dissolved in 100 mL deionized water. The mixture was evaporated at 90 ^oC until a viscous gel was obtained. Then, the mixture was heated to 180 ^oC for 3 h and calcined at 500 ^oC in the air for 5 h.

The obtained sample was denoted as $ZnZrO_x$ (1/8), where 1/8 was the molar ratio of Zn/Zr. The $ZnZrO_x$ (1/16) for STO reaction and $ZnZrO_x$ (1/100) for STA reaction were synthesized by the same method except for the Zn content. In this work, $ZnZrO_x$ was the abbreviation for three kinds of Zn-doped ZrO_2 oxide for convenience although Zn content was different unless otherwise mentioned.

The ZnO oxide was prepared by a precipitation method. The $NH_3{\cdot}H_2O$ (25 wt%) was added into the $Zn(NO_3)_2$ solution under continual stirring until the pH of the solution was 7.0. After aging for 2 h at 70°C, the precipitate was washed three times with distilled water and separated by filtration. The filter cake was dried at 100°C for 8 h and then calcined at 500°C for 5 h.

The core-shell $ZnO@SiO_2$ was prepared by a modified Stöber method. Typically, 0.5 g of ZnO was dispersed in 300 mL ethanol by sonication for 1 h followed by the addition of 2.5 mL TEOS. After stirring under 450 rpm for 4 h, 5 mL of $NH_3{\cdot}H_2O$ and 20 mL of water were added dropwise. The mixture was stirred under 450 rpm for another 4 h. Subsequently, the product was washed three times with ethanol and dried at 100°C for 8 h. The obtained sample was denoted as $ZnO@SiO_2$.

SAPO-34 and SAPO-11 zeolites were hydrothermally synthesized with various gels with the molar ratio of 3.0TEA : 0.03TEAOH : $1.0Al_2O_3$: $0.21SiO_2$: $1.0P_2O_5$: $50H_2O$ and 1 Al_2O_3:1 P_2O_5:0.3 SiO_2:1 DPA:50 H_2O, respectively[42,43]. Taking the synthesis of the SAPO-34 as an example, 4.7 g of pseudo-boehmite was dissolved in 50 mL deionized water to form alumina sol after stirring under 450 rpm for 2 h. Then 0.96 g of silica sol was added to the prepared alumina sol under stirring for 2 h. Subsequently, 14.2 g of TEA, 0.81 g of TEAOH, and 7.3 g of H_3PO_4 were added slowly under continual stirring for another 3 h until obtaining a homogeneous gel mixture. The gel mixture was sealed in a 200 mL Teflon-lined stainless-steel autoclave, followed by heating from room temperature to 200 ^oC at a rate of 2 $^oC\ min^{-1}$. The crystallization was carried out at 200 ^oC under autogenic pressure for 72 h. After crystallization, as-synthesized samples were obtained after centrifugal separation, washing, and drying at 100 ^oC for 8 h. Finally, calcination was carried out from room temperature to 550 ^oC with a rate of 2 $^oC\ min^{-1}$ and kept at 550 ^oC for 6 h to remove the organic template.

The bifunctional catalysts composed of $ZnZrO_x$ and each zeolite were prepared by five different integration manners, classified into (i) the dual-bed with the zeolite in the upstream bed and $ZnZrO_x$ oxide in the downstream bed, separated by quartz wool with 3 mm thickness, (ii) the dual-bed with $ZnZrO_x$ oxide in the upstream bed and the zeolite in the downstream bed, separated by quartz wool with 3 mm thickness, (iii) the stacking of $ZnZrO_x$ and zeolite individual granules with 30–60 meshes (grains, 250–600 μm), (iv) the stacking of $ZnZrO_x$ and zeolite individual granules with 150–200 meshes (grains, 75–100 μm), (v) the mortar-mixing for $ZnZrO_x$ and zeolite powders. They were denoted as (i) zeolite□$ZnZrO_x$, (ii) $ZnZrO_x$□zeolite (3 mm), (iii) $ZnZrO_x$ + zeolite (400 μm), (iv) $ZnZrO_x$ + zeolite (90 μm), and (v) $ZnZrO_x$/zeolite, respectively. For the syngas to lower olefins, gasoline fractions, and aromatics, SAPO-34, SAPO-11, and H-ZSM-5 were used as the zeolite component, respectively. SAPO-34, SAPO-11, ZSM-5

zeolites, and $ZnZrO_x$ oxides with low zinc content have been optimized for the above three different reactions in our previous work[42–44]. The mass ratio of $ZnZrO_x$ and the specified zeolite was fixed at 1:1. The catalysts powders were pressed, crushed, and sieved to granules of 30–60 meshes or 150–200 meshes before reaction.

Both ZnO@SiO_2/H-ZSM-5 and ZnO/H-ZSM-5 were prepared by a mortar-mixing method. ZnO-H-ZSM-5 was synthesized by an impregnation method. For these three catalysts for propylene aromatization, the weight ratio of the ZnO oxide and H-ZSM-5 zeolite was fixed at 0.015/1.

Catalyst characterization

X-ray diffraction (XRD) patterns were measured on a Rigaku Ultima IV diffractometer with Cu Kα radiation (45 kV and 30 mA) as the X-ray source. N_2 physisorption experiment was conducted on Micromeritics Tristar II 3020 Surface Area Analyzer. X-ray fluorescence (XRF) spectroscopy, which could provide information of Si/Al and Si/(Si + Al + P) ratio of zeolite, was analyzed with an S8 TIGER XRF instrument with rhodium target (50 kV, 50 mA). Scanning electron microscopy (SEM) measurements were performed on a Hitachi S-4800 operated at 15 kV.

To observe the spatial distribution of dual components for the sieved catalysts, the ultramicrotomy of resin-embedded catalysts was performed over Ultramicrotome Leica EM UC7 with a diamond knife. The catalyst granules were first embedded in Epofix resin, put in the oven overnight at 60°C, and cut to 70 nm sections using a diamond knife. Sections were deposited on a carbon-coated copper grid (300 mesh). Subsequently, transmission electron microscopy (TEM) measurements were carried out on a Phillips Analytical FEI Tecnai20 electron microscope operated at an acceleration voltage of 200 kV.

NH_3 temperature-programmed desorption (NH_3-TPD) was performed on a Micromeritics AutoChemII 2920 instrument. Typically, the sample was pretreated in a quartz reactor with purge with high-purity helium. The NH_3 adsorption was performed at 100 ^oC in an NH_3-He mixture (10 vol% NH_3) for 1 h, followed by TPD in He flow by raising the temperature to 600 ^oC at a ramp rate of 10 $^oC\ min^{-1}$. H_2 – D_2 exchange reactions were performed in a quartz reactor at 200 ^oC. Typically, 0.1 g sample was pretreated with He flow at 400 ^oC for 1 h, followed by cooling to 200 ^oC. The sample was treated in pure H_2 gas flow for 30 min. Then, pulses of high-purity D_2 were quantitatively injected into the H_2 stream. H_2 (m/z = 2), D_2 (m/z = 4), and HD (m/z = 3) were analyzed by mass spectrometry. The rate of HD formation was normalized by the specific surface area.

Catalyst evaluation

The syngas conversion was performed on a fixed-bed reactor built by Xiamen HanDe Engineering Company, Ltd. Typically, 0.6 g or 1.0 g of bifunctional catalysts was loaded in a titanium reactor (inner diameter, 8 mm). Syngas with an H_2/CO ratio of 2:1 and a pressure of 3.0 MPa was introduced into the reactor. Argon with a concentration of 4.0 vol% in the syngas was used as an internal standard for the

calculation of CO conversion. The temperature was raised to 370–400 ^{o}C at a rate of 2 ^{o}C min^{-1} to start the reaction.

The propylene aromatization was performed on the same fixed-bed reactor. Typically, 0.6 g of bifunctional catalyst was loaded in a titanium reactor. The mixture with an N_2/C_3H_6 ratio of 10/1 and a pressure of 5 bar was introduced into the reactor. The temperature was raised to 390 ^{o}C at a rate of 2 ^{o}C min^{-1} to start the reaction. Products were analyzed by an online gas chromatography equipped with a thermal conductivity detector (TCD) and two flame ionization detectors (FID). A TDX-01 packed column was connected to TCD, while RT-Q-BOND-PLOT and HP-PONA capillary columns were connected to FID. Carbon balances were all better than 95%.

Data availability

All data including supplementary materials and other findings within the article are available from the corresponding author upon reasonable request.

Declarations

Acknowledgement

This work was supported by the National Key Research and Development Program of Ministry of Science and Technology (No. 2020YFB0606401), the National Natural Science Foundation of China (Nos. 91945301, 92145301, 22121001, and 22072120), the China Postdoctoral Science Foundation (No. 2021M702733).

Author contributions

Y.L. and M.W. conducted the catalyst preparation, syngas conversion, sample characterizations by NH_3-TPD, N_2-physisorption, SEM, and XRF, and drafted the manuscript. S.L. calculated the back-mixing degree and drew all the figures in the main text. F.W. quantified the distance between two sites. S.Z. conducted the TEM analysis. Y.W. and Q.Z. contributed to the discussion of all results. K.C designed and supervised the project. All authors approved the final version of the manuscript.

Competing interests

The authors declare no competing interests.

References

1. Duyckaerts, N. *et al.* Intermediate Product Regulation in Tandem Solid Catalysts with Multimodal Porosity for High-Yield Synthetic Fuel Production. Angew. Chem. Int. Ed. **56**, 11480–11484 (2017).
2. Zhang, F. *et al.* Polyethylene upcycling to long-chain alkylaromatics by tandem hydrogenolysis/aromatization. Science **370**, 437–441 (2020).

3. Monai, M., Gambino, M., Wannakao, S. & Weckhuysen, B. M. Propane to olefins tandem catalysis: a selective route towards light olefins production. Chem. Soc. Rev. **50**, 11503–11529 (2021).
4. Yan, H. *et al.* Tandem In_2O_3-Pt/Al_2O_3 catalyst for coupling of propane dehydrogenation to selective H_2 combustion. Science **371**, 1257–1260 (2021).
5. Wang, Z., Qi, J., Yang, N., Yu, R. & Wang, D. Core-shelled Nano/Microstructures for Heterogeneous Tandem Catalysis. Mater. Chem. Front. **5**, 1126–1139 (2021).
6. Zhou, W. *et al.* New horizon in C1 chemistry: breaking the selectivity limitation in transformation of syngas and hydrogenation of CO_2 into hydrocarbon chemicals and fuels. Chem. Soc. Rev. **48**, 3193–3228 (2019).
7. Pan, X., Jiao, F., Miao, D. & Bao, X. Oxide–Zeolite-Based Composite Catalyst Concept That Enables Syngas Chemistry beyond Fischer–Tropsch Synthesis. Chem. Rev. **121**, 6588–6609 (2021).
8. Zhang, Q., Yu, J. & Corma, A. Applications of Zeolites to C1 Chemistry: Recent Advances, Challenges, and Opportunities. Adv. Mater. **32**, 2002927 (2020).
9. Vollmer, I. *et al.* Activity Descriptors Derived from Comparison of Mo and Fe as Active Metal for Methane Conversion to Aromatics. J. Am. Chem. Soc. **141**, 18814–18824 (2019).
10. Tang, P., Zhu, Q., Wu, Z. & Ma, D. Methane activation: the past and future. Energy Environ. Sci. **7**, 2580–2591 (2014).
11. Zou, S. *et al.* Surface coupling of methyl radicals for efficient low-temperature oxidative coupling of methane. Chin. J. Catal. **42**, 1117–1125 (2021).
12. Wasilke, J.-C., Obrey, S. J., Baker, R. T. & Bazan, G. C. Concurrent Tandem Catalysis. Chem. Rev. **105**, 1001–1020 (2005).
13. Yamada, Y. *et al.* Nanocrystal bilayer for tandem catalysis. Nat Chem **3**, 372–376 (2011).
14. Yang, G. H. *et al.* Oriented synthesis of target products in liquid-phase tandem reaction over a tripartite zeolite capsule catalyst. Chem. Sci. **4**, 3958–3964 (2013).
15. Kang, J. *et al.* Single-pass transformation of syngas into ethanol with high selectivity by triple tandem catalysis. Nat. Commun. **11**, 827 (2020).
16. Karim, W. *et al.* Catalyst support effects on hydrogen spillover. Nature **541**, 68–71 (2017).
17. Weisz, P. B. & Swegler, E. W. Stepwise Reaction on Separate Catalytic Centers: Isomerization of Saturated Hydrocarbons. Science **126**, 31–32 (1957).
18. Zecevic, J., Vanbutsele, G., de Jong, K. P. & Martens, J. A. Nanoscale intimacy in bifunctional catalysts for selective conversion of hydrocarbons. Nature **528**, 245–248 (2015).
19. Samad, J. E., Blanchard, J., Sayag, C., Louis, C. & Regalbuto, J. R. The controlled synthesis of metal-acid bifunctional catalysts: The effect of metal:acid ratio and metal-acid proximity in Pt silica-alumina catalysts for n-heptane isomerization. J. Catal. **342**, 203–212 (2016).
20. Lin, T. *et al.* Direct Production of Higher Oxygenates by Syngas Conversion over a Multifunctional Catalyst. Angew. Chem. Int. Ed. **58**, 4627–4631 (2019).

21. Wang, Y. *et al.* Direct Conversion of CO_2 to Ethanol Boosted by Intimacy-Sensitive Multifunctional Catalysts. ACS Catal. **11**, 11742–11753 (2021).
22. Weisz, P. B. Diffusion and Chemical Transformation. Science **179**, 433–440 (1973).
23. Jiang, H., Hou, Z. & Luo, Y. A Kinetic View on Proximity-Dependent Selectivity of Carbon Dioxide Reduction on Bifunctional Catalysts. ACS Catal. **10**, 13518–13523 (2020).
24. Cheng, K. *et al.* Impact of the Spatial Organization of Bifunctional Metal-Zeolite Catalysts for Hydroisomerization of Light Alkanes. Angew. Chem. Int. Ed. **59**, 3592–3600 (2020).
25. Ding, Y. *et al.* Effects of Proximity-Dependent Metal Migration on Bifunctional Composites Catalyzed Syngas to Olefins. ACS Catal. **11**, 9729–9737 (2021).
26. Wang, Y. *et al.* Visualizing Element Migration over Bifunctional Metal-Zeolite Catalysts and its Impact on Catalysis. Angew. Chem. Int. Ed. **60**, 17735–17743 (2021).
27. Jiao, F. *et al.* Selective conversion of syngas to light olefins. Science **351**, 1065–1068 (2016).
28. Cheng, K. *et al.* Direct and Highly Selective Conversion of Synthesis Gas to Lower Olefins: Design of a Bifunctional Catalyst Combining Methanol Synthesis and Carbon–Carbon Coupling. Angew. Chem. Int. Ed. **55**, 4725–4728 (2016).
29. Wei, J., Yao, R., Han, Y., Ge, Q. & Sun, J. Towards the development of the emerging process of CO2 heterogenous hydrogenation into high-value unsaturated heavy hydrocarbons. Chem. Soc. Rev. **50**, 10764–10805 (2021).
30. Wang, D., Xie, Z., Porosoff, M. D. & Chen, J. G. Recent advances in carbon dioxide hydrogenation to produce olefins and aromatics. Chem **7**, 2277–2311 (2021).
31. Zuo, J. *et al.* Selective methylation of toluene using CO2 and H2 to para-xylene. Sci. Adv. **6**, eaba5433 (2020).
32. Gao, P., Zhang, L., Li, S., Zhou, Z. & Sun, Y. Novel Heterogeneous Catalysts for CO_2 Hydrogenation to Liquid Fuels. ACS Cent. Sci. **6**, 1657–1670 (2020).
33. Bao, J., Yang, G., Yoneyama, Y. & Tsubaki, N. Significant Advances in C1 Catalysis: Highly Efficient Catalysts and Catalytic Reactions. ACS Catal. **9**, 3026–3053 (2019).
34. Tan, L. *et al.* Design of the core-shell catalyst: an effective strategy for suppressing side reactions in syngas to light olefins direct selective conversion. Chem. Sci. **11**, 4097–4105 (2020).
35. Chen, J. *et al.* Hydrogenation of CO_2 to light olefins on CuZnZr@(Zn-)SAPO-34 catalysts: Strategy for product distribution. Fuel **239**, 44–52 (2019).
36. Xie, C. *et al.* Tandem Catalysis for CO_2 Hydrogenation to C_2–C_4 Hydrocarbons. Nano Lett. **17**, 3798–3802 (2017).
37. Xiao, J. *et al.* Tandem catalysis with double-shelled hollow spheres. Nat. Mater. (2022).
38. Gao, P. *et al.* Direct conversion of CO_2 into liquid fuels with high selectivity over a bifunctional catalyst. Nat. Chem. **9**, 1019–1024 (2017).
39. Wei, J. *et al.* Directly converting CO_2 into a gasoline fuel. Nat. Commun. **8**, 15174 (2017).

40. Ni, Y. *et al.* Realizing and Recognizing Syngas-to-Olefins Reaction via a Dual-Bed Catalyst. ACS Catal. **9**, 1026–1032 (2019).
41. Dokania, A. *et al.* Designing a Multifunctional Catalyst for the Direct Production of Gasoline-Range Isoparaffins from CO_2. JACS Au **1**, 1961–1974 (2021).
42. Wang, M. *et al.* Synthesis of hierarchical SAPO-34 to improve the catalytic performances of bifunctional catalysts for syngas-to-olefins reaction. J. Catal. **394**, 181–192 (2021).
43. Wang, M. *et al.* Effect of zeolite topology on the hydrocarbon distribution over bifunctional ZnAlO/SAPO catalysts in syngas conversion. Catal. Today **371**, 85–92 (2021).
44. Cheng, K. *et al.* Bifunctional Catalysts for One-Step Conversion of Syngas into Aromatics with Excellent Selectivity and Stability. Chem **3**, 334–347 (2017).
45. Liu, X. *et al.* Design of efficient bifunctional catalysts for direct conversion of syngas into lower olefins via methanol/dimethyl ether intermediates. Chem. Sci. **9**, 4708–4718 (2018).
46. Xu, S. *et al.* Advances in Catalysis for Methanol-to-Olefins Conversion. Adv. Catal. **61**, 37–122 (2017).
47. Li, Y. *et al.* Highly Selective Conversion of Syngas to Higher Oxygenates over Tandem Catalysts. ACS Catal. **11**, 14791–14802 (2021).
48. Huysmans, M. & Dassargues, A. Review of the use of Péclet numbers to determine the relative importance of advection and diffusion in low permeability environments. Hydrogeol. J. **13**, 895–904 (2005).
49. LeViness, S., Deshmukh, S. R., Richard, L. A. & Robota, H. J. Velocys Fischer–Tropsch Synthesis Technology—New Advances on State-of-the-Art. Top. Catal. **57**, 518–525 (2014).
50. Hernández Mejía, C., van Deelen, T. W. & de Jong, K. P. Activity enhancement of cobalt catalysts by tuning metal-support interactions. Nat. Commun. **9**, 4459 (2018).
51. Iglesia, E. & Baumgartner, J. E. Hydrogen transfer and activation of propane and methane on ZSM5-based catalysts. Catal. Lett. **21**, 55–70 (1993).
52. Biscardi, J. A. & Iglesia, E. Structure and function of metal cations in light alkane reactions catalyzed by modified H-ZSM5. Catal. Today **31**, 207–231 (1996).
53. van Deelen, T. W., Hernández Mejía, C. & de Jong, K. P. Control of metal-support interactions in heterogeneous catalysts to enhance activity and selectivity. Nat. Catal. **2**, 955–970 (2019).
54. Chen, X. *et al.* Influence of Zn species in HZSM-5 on ethylene aromatization. Chin. J. Catal. **36**, 880–888 (2015).
55. Senger, S. & Radom, L. Zeolites as Transition-Metal-Free Hydrogenation Catalysts: A Theoretical Mechanistic Study. J. Am. Chem. Soc. **122**, 2613–2620 (2000).
56. Shi, Z., Neurock, M. & Bhan, A. Methanol-to-Olefins Catalysis on HSSZ-13 and HSAPO-34 and Its Relationship to Acid Strength. ACS Catal. **11**, 1222–1232 (2021).
57. Guisnet, M., Gnep, N. S. & Alario, F. Aromatization of short chain alkanes on zeolite catalysts. Appl. Catal. A **89**, 1–30 (1992).

58. Iglesia, E., Barton, D. G., Biscardi, J. A., Gines, M. J. L. & Soled, S. L. Bifunctional pathways in catalysis by solid acids and bases. Catal. Today **38**, 339–360 (1997).

Figures

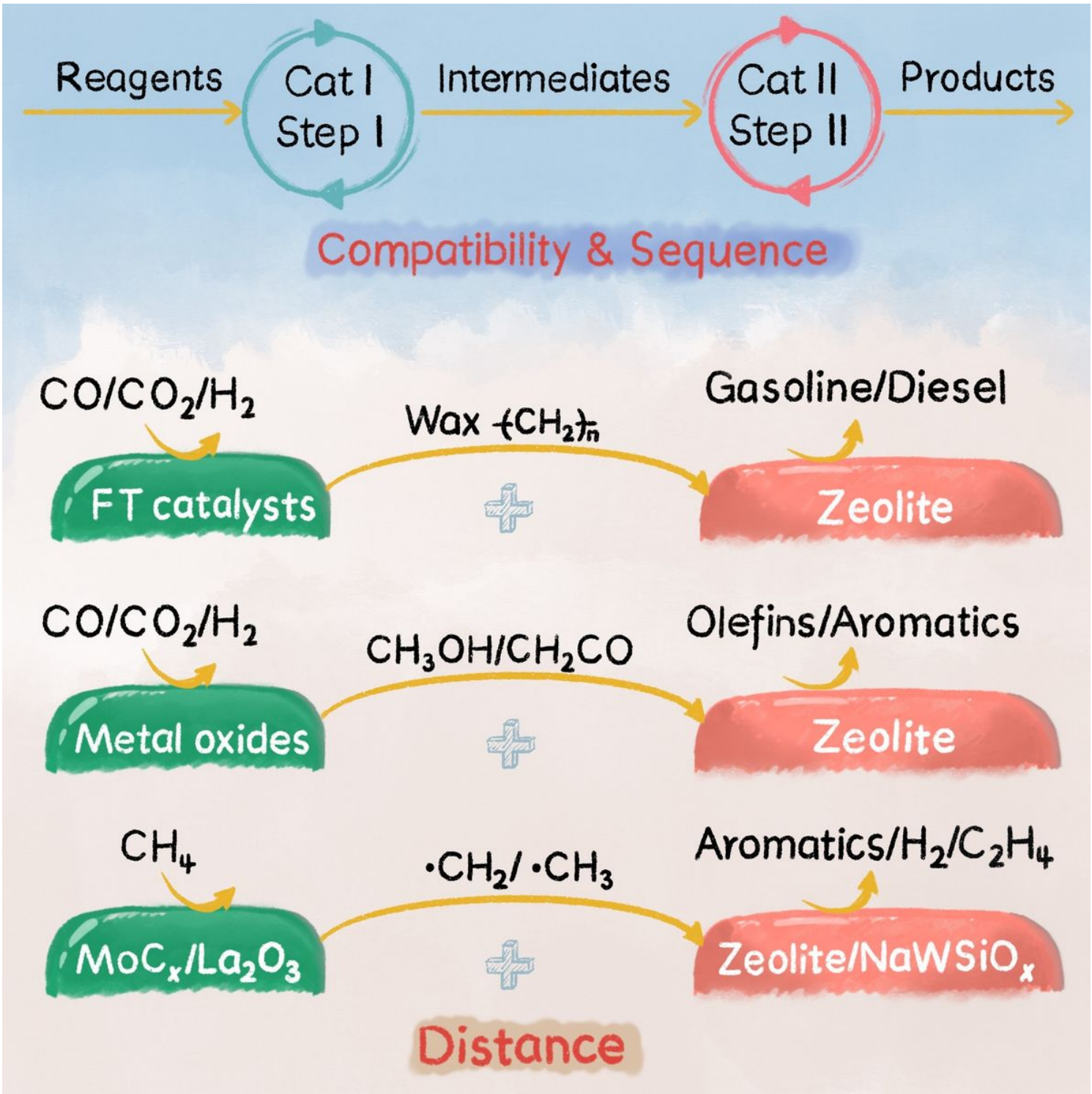

Figure 1

Illustration of tandem catalysis and representative advances in C1 chemistry. Because the metal functions for activating C1 molecules are diverse, the reaction intermediates can be large molecules (such as wax produced by Fischer-Tropsch synthesis), small molecules (such as methanol and ketone), and small radicals (such as methyl and methylene).

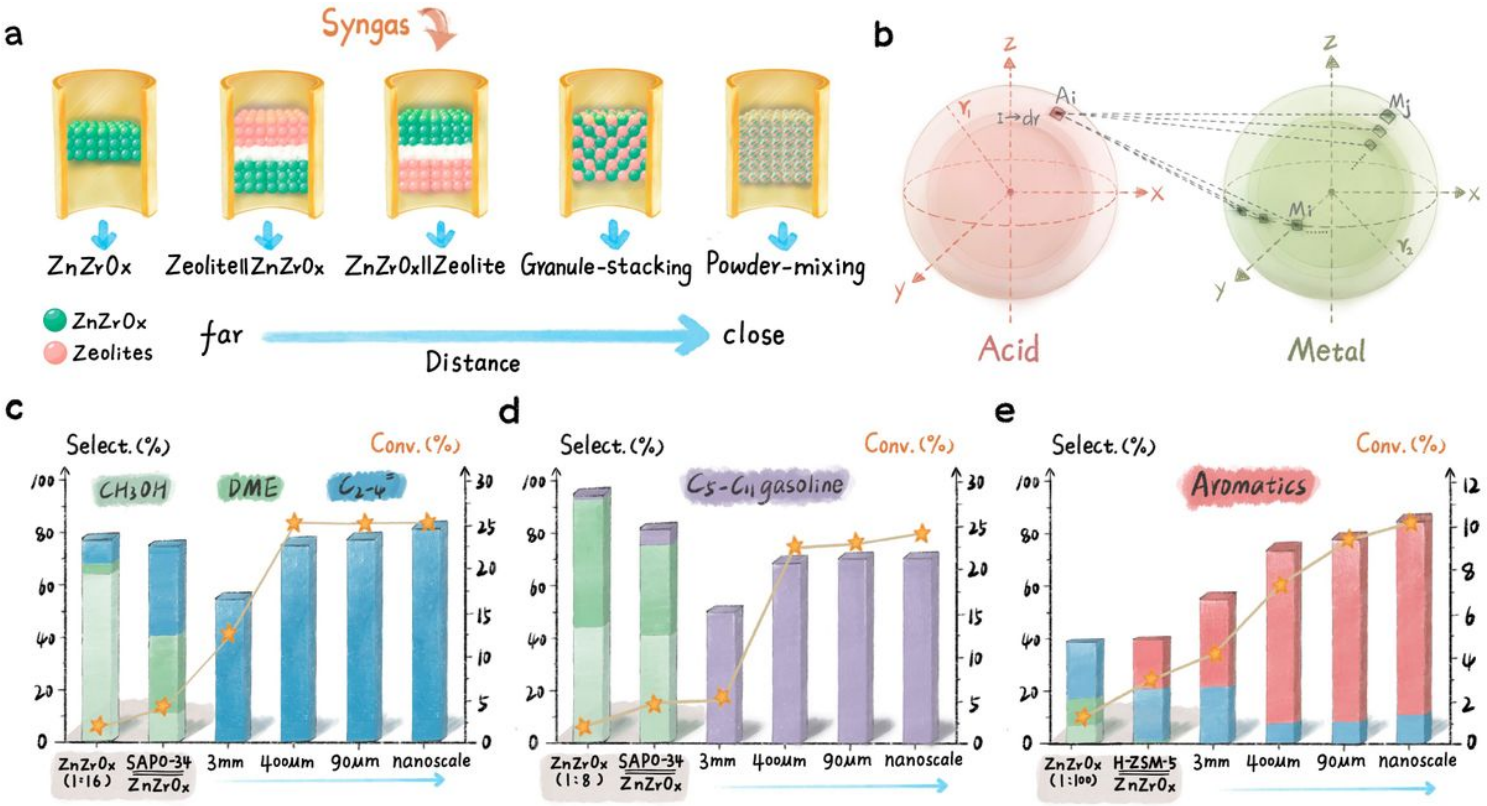

Figure 2

The effect of distance between $ZnZrO_x$ and zeolites on the performance of syngas conversion. a Integration manners from left to right: $ZnZrO_x$; dual-bed zeolite||$ZnZrO_x$; dual-bed $ZnZrO_x$||zeolite; $ZnZrO_x$+zeolite with an approximate distance of 400 or 90 μm, respectively, by stacking individual granules with different sizes; and $ZnZrO_x$/zeolite prepared by the powder-mixing method. **b** The scheme of the iterative method for distance estimation between $ZnZrO_x$ and zeolite. **c** STO performance. **d** STG performance. **e** STA performance. Reaction condition: W_{cat} = 0.6 g or 1 g, H_2/CO = 2, P = 3 MPa, time on stream = 10 h. The Zn/Zr ratios for STO, STG, and STA reactions are 1/16, 1/8, and 1/100, respectively. Details for distance estimation and reaction conditions can be found in Supplementary Tables 3–5.

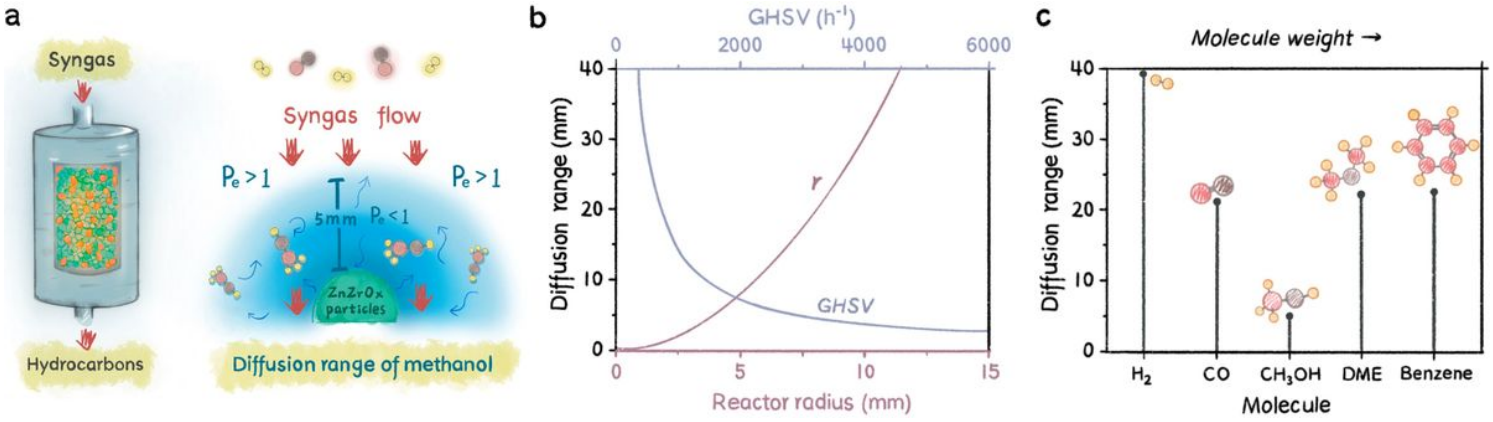

Figure 3

Evaluation of back-mixing degree. a Schematic diagram of diffusional behaviors in a typical fixed-bad reactor and the diffusion distance of methanol assessed by Péclet number. **b** The effect of reactor diameter and gas space velocity on the diffusion range of methanol. **c** The dependence of gas diffusivity on molecule type. The calculation and assumption details can be found in the Supplementary Information.

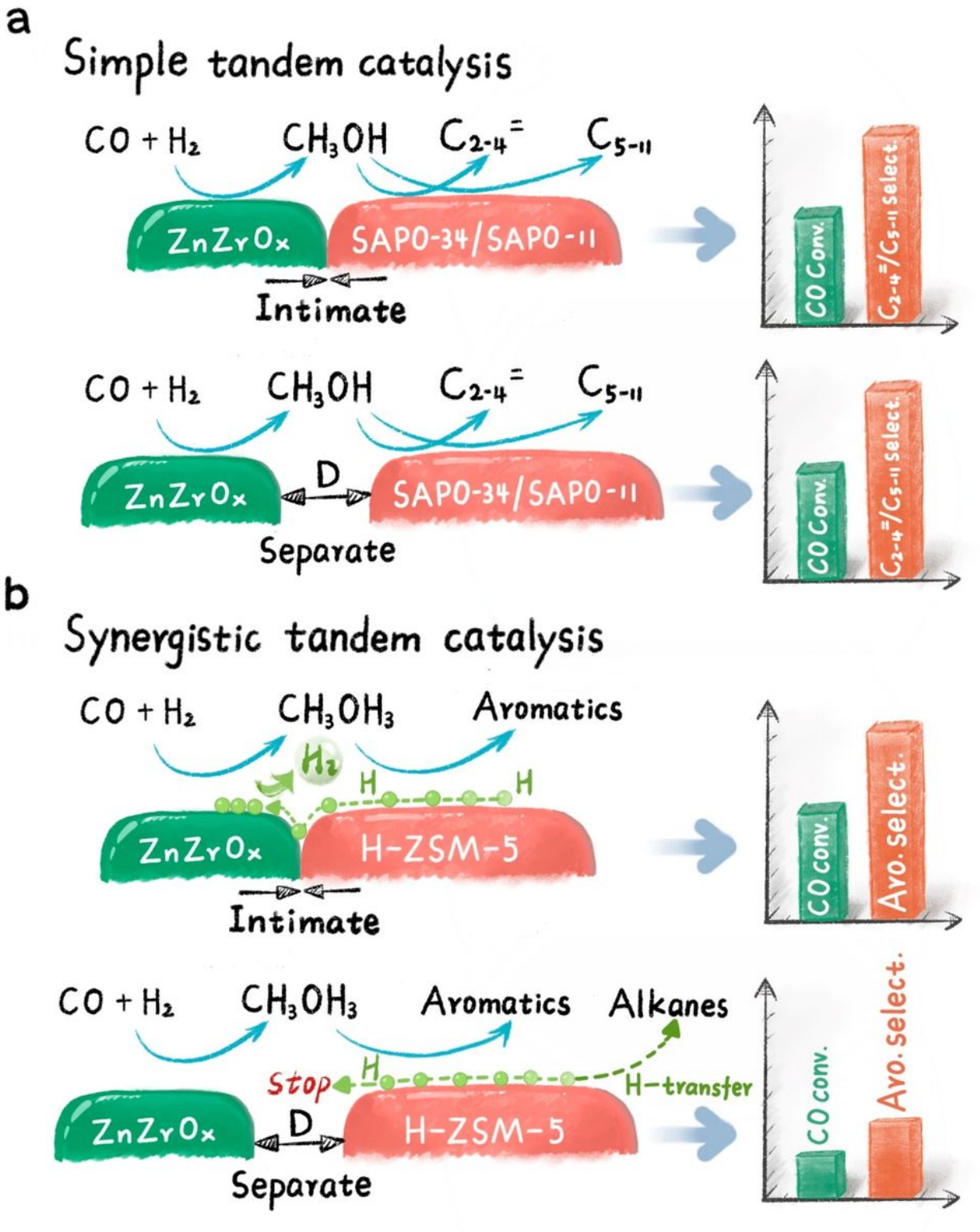

Figure 4

The distance required for efficient communication between $ZnZrO_x$ and zeolites. a STO and STG reactions with flexible distance requirements. **b** STA reaction with necessary intimate contact for removing hydrogen species.

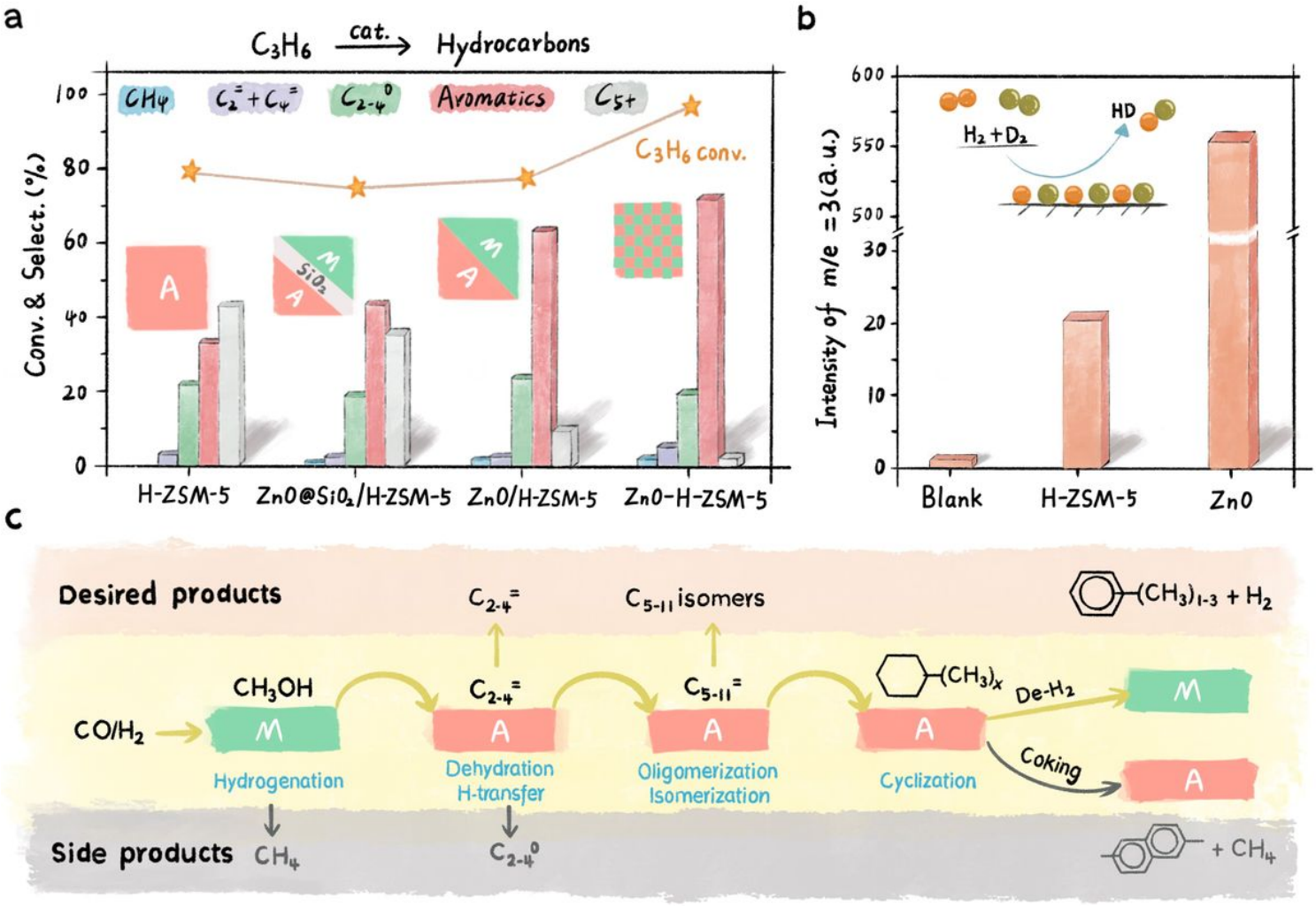

Figure 5

Probe experiments and reaction network. a The dependence of distance between ZnO and H-ZSM-5 on C_3H_6 aromatization. Reaction conditions: W_{cat} = 0.6 g, F_{N2} = 15 mL min^{-1}, F_{C3H6} = 1.5 mL min^{-1}, T = 390 ^oC, P = 5 bar, time on stream = 4 h. **b** H-D exchange over blank quatz reator, H-ZSM-5, and ZnO. The HD intensity was normalized to the surface area. **c** Reaction network for the selective conversion of syngas into desired olefins, gasoline, and aromatics. De-H_2 denotes dehydrogenation. Some possible side products are also presented.

Supplementary Files

This is a list of supplementary files associated with this preprint. Click to download.

- SupplementaryInformation.docx